Available online at www.sciencedirect.com
ScienceDirect
Geochimica et Cosmochimica Acta 70 (2006) 4725–4733
Geochimica
www.elsevier.com/locate/gca

Direct dating of hydrothermal W mineralization: U–Pb age for hübnerite ($MnWO_4$), Sweet Home Mine, Colorado

Rolf L. Romer *, Volker Lüders

GeoForschungsZentrum Potsdam, Telegrafenberg, D-14473 Potsdam, Germany

Received 17 January 2006; accepted in revised form 6 July 2006

Abstract

We have investigated the potential of hübnerite for U–Pb dating. Hübnerite forms typically at medium to low-temperatures in a wide range of pneumatolytic-hydrothermal mineral deposits, particularly porphyry molybdenum and Sn-specialized granites. Hübnerite from the Sweet Home Mine (Alma, Colorado) formed in a Pb-rich, U-poor environment, but still developed relatively radiogenic Pb isotopic compositions. The low Pb_{common} contents in hübnerite (0.075 to 0.155 ppm) demonstrate that Pb is efficiently excluded from the crystal lattice. In contrast, U may substitute for Mn. The U–Pb data of hübnerite scatter. Most of the scatter originates from samples with $^{206}Pb/^{204}Pb$ values below 50, where Pb_{blank} contributes up to 30% to Pb_{total}. Using the least radiogenic galena Pb, samples with $^{206}Pb/^{204}Pb$ values above 70 have overlapping $^{206}Pb*/^{238}U$ and $^{207}Pb*/^{235}U$ values and yield a $^{206}Pb/^{238}U$ age of 25.7 ± 0.3 Ma (2σ). Late stage apatite from the Sweet Home Mine yields a $^{206}Pb/^{204}Pb$–$^{238}U/^{204}Pb$ isochron corresponding to an age of 24.8 ± 0.5 Ma (2σ). A comparison of the U–Pb hübnerite ages with literature $^{40}Ar/^{39}Ar$ ages on earlier sericite and the U–Pb age on later apatite suggests that (i) hübnerite yields accurate U–Pb ages and (ii) the evolution of the Sweet Home mineralization from greisen-type mineralization to medium-temperature hydrothermal vein mineralization took place in a few hundred thousand years at most. Aqueous low-N_2-bearing and aqueous inclusions in the dated hübnerite have homogenization temperatures between 325 and 356 °C and moderate salinity (up to 6.7 wt% NaCl equiv.). Thus, hübnerite represents one of the rare examples of a mineral that can be dated accurately and carries petrological information.

1. Introduction

One of the major ambiguities in geochronology originates from the linking of age data with petrological parameters. This problem is particularly important for metamorphic rocks, where precise and accurate age data must be linked through mineral reactions to pressure and temperature conditions (e.g., Möller et al., 2003) and are then used to derive rates of cooling, exhumation, mineral growth, and deformation. The ambiguity was resolved in part by dating minerals used to define P–T conditions (e.g., Christensen et al., 1989; Vance and O'Nions, 1990; Burton and O'Nions, 1991; Duchène et al., 1997; Romer and Rötzler, 2001; Baxter, 2003), although daughter-element inheritance from precursor minerals may result in inaccurate ages (e.g., Romer, 2001; Romer and Rötzler, 2003; Romer and Siegesmund, 2003; Romer and Xiao, 2005). The problem of linking age data with petrological data is even more obvious in low-temperature hydrothermal systems, as there are only a few geochronometers available to date such systems, e.g., $^{40}Ar/^{39}Ar$, K–Ar, and Rb–Sr on white mica (e.g., Franzke et al., 1996; Macfarlane et al., 1999; Kontak and Archibald, 2002), U–He on hematite (Wernicke and Lippolt, 1993, 1994), and more recently U–Pb on opal and chalcedony (Neymark et al., 2000) and agate (Romer and Linnemann, 2004). For hydrothermal deposits, however, the petrological information is generally derived from fluid inclusions in minerals (e.g., quartz, calcite) other than the dated ones.

Minerals that can be dated directly and that carry fluid inclusions accessible to observation, i.e., the host is

* Corresponding author. Fax: +49 331 288 1474.
E-mail address: romer@gfz-potsdam.de (R.L. Romer).

0016-7037/$ - see front matter © 2006 Elsevier Inc. All rights reserved.
doi:10.1016/j.gca.2006.07.003

transparent to light in the visible or the near IR spectral range, provide the best possibility to link unambiguously age and petrologic information. Such an approach has been taken by Lüders et al. (2005) and Romer et al. (2005b) who dated fluid inclusions in hematite from jacutinga-type Pd–Pt–Au mineralizations of the Quadrilátero Ferrífero (Brazil) and performed micro-chemistry and fluid inclusion studies on the same material. A similar approach was taken earlier by Pettke and Diamond (1995, 2000) who used the Rb–Sr systematics of fluid inclusions in quartz and sphalerite to infer the age of hydrothermal formations. In this paper, we present for the first time U–Pb data from hydrothermal hübnerite. Hübnerite is known to be transparent to infrared light and, thus, suitable for fluid inclusion studies (Lüders, 1996; Bailly et al., 2002). The fluid inclusions carry information about the composition of the fluid in terms of major constituents and dissolved components, which in combination with the trapping conditions allows to constrain the evolution history of the fluid and to deduce its possible source. The dating of the same minerals places an age constraint on these specific conditions. Extending this approach to a polystage hydrothermal system and performing fluid inclusion and dating studies on an entire range of minerals from different evolution stages of the hydrothermal system would allow evaluation of its geochemical development through time.

2. Hübnerite from the Sweet Home Mine (Alma mining district, Colorado)

The Sweet Home Mine, located in the Alma mining district on the eastern slope of central Colorado's Mosquito Range (Fig. 1), was mined for silver in the 19th century. The mineralization of the Sweet Home Mine is hosted by Precambrian igneous and metamorphic rocks and minor Tertiary porphyric dikes and pegmatites. Paragenetically, two distinct stages are observed in the mine, an early, high-temperature mineral assemblage containing quartz–muscovite–pyrite–topaz–molybdenite–fluorite, and a later, lower temperature assemblage containing galena–sphalerite–tetrahedrite–bornite and other sulfides/sulfosalts, and fluorite–rhodochrosite. Hydrothermal activity ended with the precipitation of apatite, calcite, and minor barite. Within the mine three major steeply dipping structural fault systems, striking WNW, NE, and N, can be distinguished (Misantoni et al., 1998). These structures contain altered Tertiary porphyritic intrusions and all stages of mineralization indicating their pre-existence to mineralization. However, most of the Ag-bearing sulfide mineralization occurs on NE trending faults (Misantoni et al., 1998).

Tungsten mineralization, in the form of hübnerite, is common, but it is not clear whether it is associated with the early mineralization stage. It may in fact be transitional

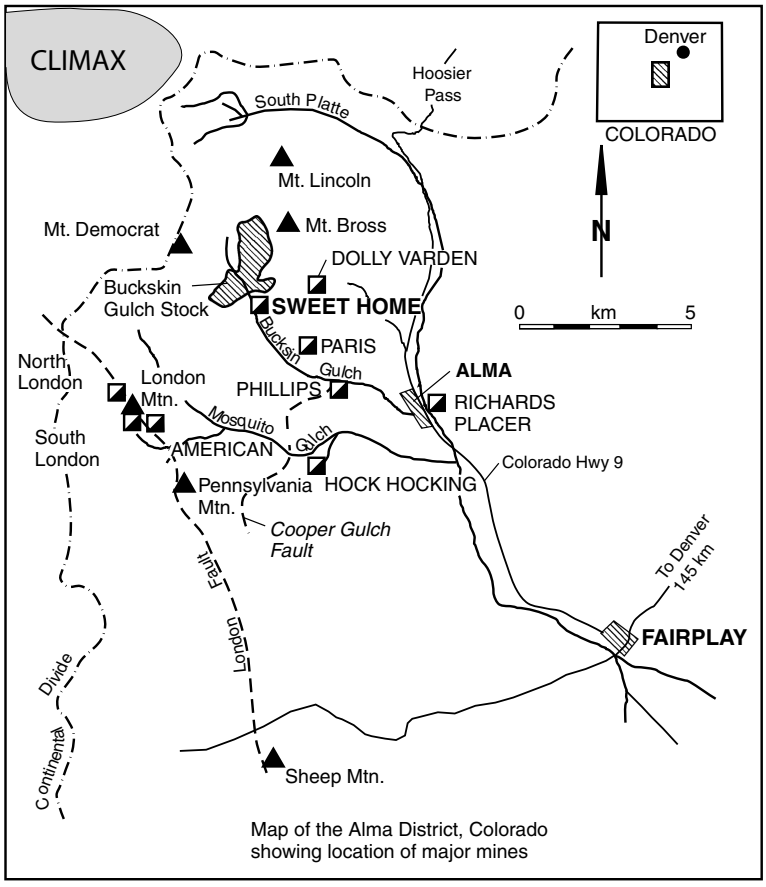

Fig. 1. Simplified location map of the Alma mining district and the Sweet Home Mine (Moore, 1998). Note that the Alma mining district lies within the Colorado Mineral Belt and that the Sweet Home Mine is less than 8 km from the Climax porphyry molybdenum deposit.

between the two main stages. It is irregularly distributed in the mined area and generally forms blades with and on needle quartz and is associated with sulfides, rhodochrosite, and fluorite (Fig. 2A). Single blades of hübnerite are as long as 3 cm (Murphy and Hurlbut, 1998). Locally, hübnerite is followed by pyrite, muscovite, and topaz. Rhodochrosite grows on needle quartz and where present also on hübnerite. There is rare gem-clear cherry-red rhodochrosite and pale-pink, typically cloudy rhodochrosite. The cherry-red rhodochrosite is older than the cloudy rhodochrosite and formed at temperatures around 300–325 °C (Reynolds, 1998). It has fewer solid and fluid inclusions than the cloudy rhodochrosite and has low contents of Fe (+ Mg + Ca) (Wenrich, 1998). In contrast, the younger pale-pink rhodochrosite is rich in inclusions of topaz, apatite, and fluid inclusions (Wenrich, 1998), that homogenize at temperatures ranging from around 200 °C to as low as 145–135 °C (Reynolds, 1998). This cloudy pale-pink rhodochrosite has high contents of Fe (+ Mg + Ca), i.e., up to c. 9 wt% FeO (Wenrich, 1998). Rhodochrosite is followed by fluorite, which is characterized by aqueous fluid inclusions that homogenize at temperatures of 150 to 110 °C (Reynolds, 1998), and fluorapatite.

Primary two-phase fluid inclusions in hübnerite samples of the Sweet Home Mine are always oriented along the growth direction, i.e., parallel to {100} or {010}, and are irregular in shape. They are typically 30–60 μm long (Fig. 2B). During freezing runs, most fluid inclusions in hübnerite show melting of ice at around −5 °C and melting of clathrate between 3.6 and 3.8 °C. Laser Raman spectroscopy proves the exclusive presence of dissolved nitrogen in these aqueous inclusions (Fig. 2C). An estimate of the salinity is derived from two-phase inclusions in hübnerite samples that host N_2-free aqueous inclusions yielding salinity between 5.7 and 6.3 wt% equivalent. In the system N_2–H_2O, clathrates of nitrogen form at about 250 bar at 3.6–3.8 °C (Jhaveri and Robinson, 1965). Since the salt content of the ore-forming fluid is moderate, this pressure estimate may be realistic for the conditions of fluid entrapment and the homogenization temperatures of both types of inclusions, which lie between 325 and 355.6 °C, are close to the true trapping conditions. The presence of nitrogen in some hübnerite-hosted inclusions is unusual as fluid inclusions in quartz, rhodochrosite, and some early fluorite crystals contain small amounts of CO_2 but no N_2.

3. Analytical procedures

The top part of a single 2 × 2 × 18 mm large hübnerite crystal was broken into small pieces. Individual fragments selected for dating were checked under the binocular microscope to be free of surface alterations, fractures, and visible intergrowths. The hübnerite samples were washed in warm 7 N HNO_3, H_2O, and acetone. A mixed ^{205}Pb–^{235}U tracer was added before sample dissolution. Samples were dissolved in 40% HF overnight, using closed screw-top teflon vials on the hot plate at 160 °C. The

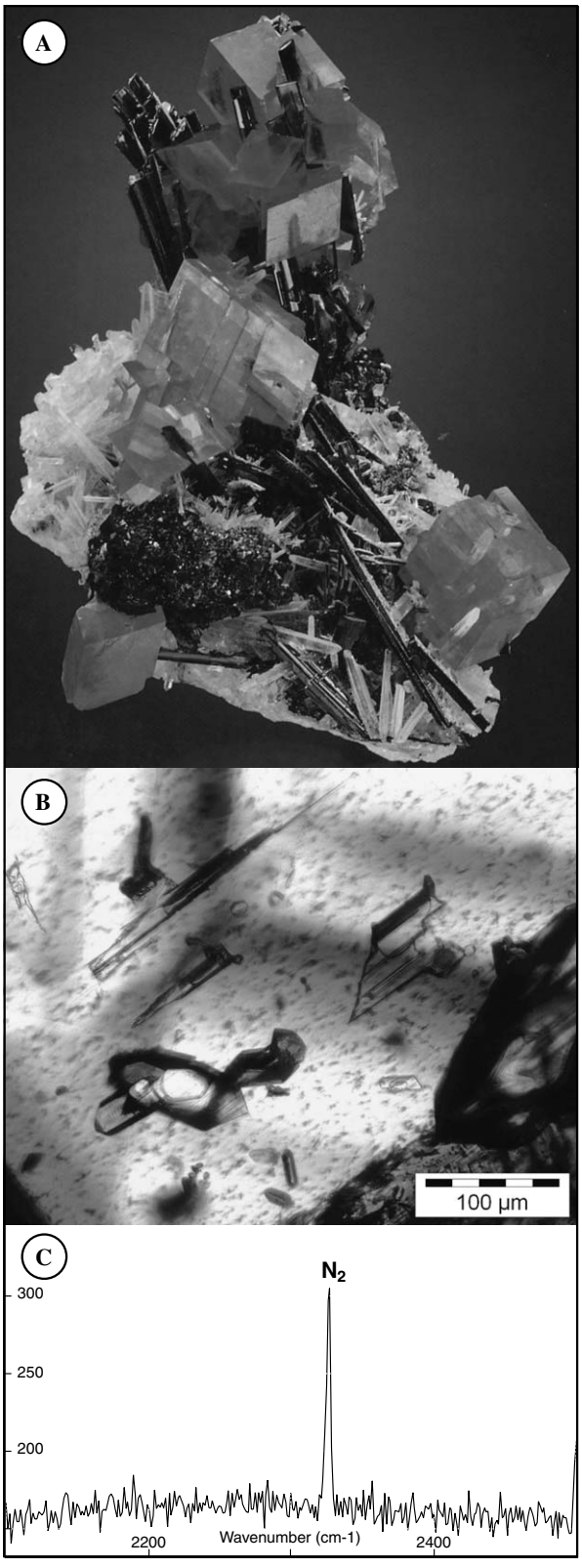

Fig. 2. (A) Typical appearance of hübnerite in Sweet Home Mine. Hübnerite forms distinctive needles on a carpet of white to colorless quartz and is overgrown by pink rhodochrosite crystals. Photo courtesy of Jeff Scovil. Hübnerite has formed early in the hydrothermal mineral assemblage. (B) Fluid inclusion in hübnerite. (C) Raman spectrum of N_2-bearing inclusion in hübnerite.

perfectly clear solution was dried slowly at 90 °C. The sample was then transformed into chloride form using 6 N HCl. The dried sample was taken up in 3 N HCl for ion-exchange chromatography using Biorad AG1-X8 anion-exchange resin (cf. Romer et al., 2005a). In HCl, elongate yellow crystals precipitated that did not redissolve. As sample and tracer homogenized in HF, and U and Pb apparently were not scavenged to a significant extent by these precipitates, the yellow crystals did not compromise the ion-exchange chemistry. Instead, they even reduced the ion-charge on the columns. The apatite samples were broken from the top part of single crystal, separated under the binocular, and washed in alcohol, H_2O, and acetone. A mixed ^{205}Pb–^{235}U tracer was added before sample dissolution. Samples were dissolved in 7 N HNO_3 and then transformed into chloride form. Lead and U were purified using the same procedure as for hübnerite samples.

The isotopic composition of Pb and U was determined using a Finnigan MAT262 multi-collector mass-spectrometer. Pb and U were loaded with dilute H_3PO_4 and silica gel on separate Re single-filaments. Lead was analyzed at 1200–1260 °C, U at 1300–1360 °C. U and Pb were analyzed using static multi-collection. The hübnerite samples were analyzed using a SEM and Faraday collectors, the Pb-rich apatite samples were analyzed using Faraday collectors. All isotope ratios were corrected for isotopic fractionation of 0.1%/a.m.u. as determined from the repeated analysis of Pb reference material NBS 981, 15 pg Pb blank, 1 pg U blank, and tracer Pb contribution.

All uncertainties (concentrations, isotopic ratios, and ages) were estimated using a Monte-Carlo simulation with the following uncertainties: measurement errors, 30% uncertainty for the correction of mass fractionation, 50% uncertainty of the amount of blank Pb and U, 0.1, 0.05, 0.2 absolute uncertainty for $^{206}Pb/^{204}Pb$, $^{207}Pb/^{204}Pb$, and $^{208}Pb/^{204}Pb$ of the blank and initial Pb composition, respectively, tracer Pb contribution ($^{205}Pb/^{206}Pb = 21.693$), and 0.3% for the $^{205}Pb/^{235}U$ ratio of the mixed tracer. Data reduction was performed by Monte-Carlo modeling of 1000 random normally distributed data sets that fit above uncertainty limits, allowing for error correlation when appropriate.

4. U–Pb isotope data

4.1. Hübnerite

Hübnerite is a monoclinic tungsten manganese oxide ($MnWO_4$) that forms solid solutions with ferberite ($FeWO_4$). Typically, it occurs in medium to low temperature hydrothermal mineral deposits, pneumatolytically altered granites and greisens, and granite pegmatites (e.g., Wood and Samson, 2000). Nb, Ta, and Sn may substitute for the sixfold coordinated W, whereas Sc, Fe, and Zn may substitute for sixfold coordinated Mn. Charge balance for Nb and Ta may be obtained by coupled substitution (Fe, $Mn)^{2+} + W^{6+} \leftrightarrow (Fe, Sc)^{3+} + (Nb, Ta)^{5+}$ (e.g., Cerny and Ercit, 1989). Similar coupled exchange may also account for the incorporation of REE^{3+} and U^{6+}. This substitution of REE into wolframite-series minerals was exploited in several attempts to data this mineral by the ^{147}Sm–^{143}Nd method (e.g., Belyatsky et al., 1993; Nie et al., 2002). Due to the relatively limited range in $^{147}Sm/^{144}Nd$ values, these ages have relatively large uncertainties and—at least locally—gave anomalously old isochron ages.

Crystal chemical consideration indicate that Pb is unlikely to be incorporated in the crystal lattice of hübnerite, as the ionic radius of Pb^{2+} (1.21 Å, Shannon, 1976) is too large to fit into the W octahedral (0.60 Å) or Mn octahedral sites (0.83 Å). In contrast, U^{4+} and U^{6+} have much smaller ionic radii and higher charges, which makes U much more likely than Pb to be incorporated in the crystal lattice of hübnerite. To our knowledge, there are no investigations on the valence of U in hübnerite. Octahedrally coordinated U^{6+} and U^{4+} have ionic radii of 0.73 and 0.89 Å, respectively. Since octahedrally coordinated Fe^{2+} and Mn^{2+} that have ionic radii of 0.78 Å and 0.83 Å (Shannon, 1976), respectively, U may substitute in the site of Fe^{2+} and Mn^{2+} independent of its oxidation stage by coupled substitution. Thus, it may be anticipated that hübnerite develops a highly radiogenic Pb isotopic composition with time even if the total contents of U are relatively low.

We analyzed eight hübnerite fragments. $^{206}Pb/^{204}Pb$ values of individual fragments fall in the range from 38.3 to 120.1 (Table 1). The amount of Pb_{common} in the dated hübnerite fragments ranges from 17 to 40 pg (total amount of Pb ranges from 46 to 105 pg), which for sample weights of 0.346 to 0.929 mg corresponds to Pb_{common} contents of 0.076 to 0.155 ppm. Because of the low total amount of Pb in each sample, 5 to 30% of the Pb_{total} originates from the blank (c. 7 to 20 pg Pb, possibly of different composition for individual samples). Thus, especially for samples with low measured $^{206}Pb/^{204}Pb$ values, the amount and isotopic compositions of blank and initial Pb significantly influence the calculated amount of radiogenic Pb. U contents are markedly higher than those of Pb and fall in the range of 6.30 to 30.4 ppm (Table 1).

The best age estimate is obtained from those samples with the highest measured $^{206}Pb/^{204}Pb$ as these are least sensitive to uncertainties from the corrections of blank and common Pb. Apparent $^{206}Pb/^{238}U$ ages of the eight hübnerite fractions range from 24.2 ± 0.2 to 29.2 ± 0.2 Ma (2σ, Table 1). The three samples with the highest $^{206}Pb/^{204}Pb$, however, yield $^{206}Pb/^{238}U$ ages overlapping within error in the range from 25.5 to 25.9 Ma. The data fall slightly to the right of the concordia curve (Fig. 3a). This may be due to the Pb_{common} correction based on the least radiogenic galena–Pb from the Sweet Home Mine (Table 1). The use of a different Pb isotopic composition for blank Pb, a more radiogenic Pb isotopic composition for initial Pb, or a change in the relative importance of blank and initial Pb shifts the three samples with the highest $^{206}Pb/^{204}Pb$ values to lower $^{207}Pb^*/^{235}U$ values, i.e., onto the concordia. Samples with lower

Table 1
U–Pb analytical results for hübnerite from the Sweet Home Mine, Colorado

	Weight (mg)	Concentrations (ppm)		Measured ratios[b]				Radiogenic Pb (at%)[d]			Atomic rations[d]				Apparent ages (Ma)[e]	
		U	Pb	$^{206}Pb/^{204}Pb$	$^{207}Pb/^{204}Pb$	$^{238}U/^{204}Pb$	Pb_{total}[c] (pg)	^{206}Pb	^{207}Pb	^{208}Pb	$^{206}Pb/^{238}U$	$^{207}Pb/^{235}U$	$^{207}Pb/^{206}Pb$	Rho	$^{206}Pb/^{238}U$	$^{207}Pb/^{235}U$
H1[a]	0.428	15.7	0.097	70.21 (34)	18.10 (9)	13100	56.6	95.27	4.57	0.16	.00396 (2)	.0262 (10)	.0480 (17)	0.37	25.5 ± 0.1	26.3 ± 1.0
H2	0.346	10.4	0.149	37.11 (16)	16.72 (7)	4350	66.8	94.30	5.51	0.19	.00437 (4)	.0352 (26)	.0584 (40)	0.48	28.1 ± 0.3	35.1 ± 2.5
H3	0.362	7.98	0.084	39.46 (20)	16.79 (9)	5300	45.6	92.56	5.17	2.27	.00402 (4)	.0310 (26)	.0559 (44)	0.43	25.9 ± 0.3	31.0 ± 2.5
H4	0.374	10.3	0.100	41.57 (26)	16.83 (11)	6200	52.4	94.65	4.94	0.41	.00377 (3)	.0271 (34)	.0522 (63)	0.49	24.2 ± 0.2	27.2 ± 3.3
H5	0.543	8.12	0.104	39.16 (13)	16.82 (6)	5100	71.4	93.97	5.41	0.62	.00413 (3)	.0328 (18)	.0575 (30)	0.41	26.6 ± 0.2	32.7 ± 1.8
H6	0.634	6.30	0.076	42.70 (28)	16.93 (11)	5400	63.0	95.59	5.17	0.00	.00455 (4)	.0339 (30)	.0541 (46)	0.62	29.2 ± 0.2	33.9 ± 3.0
H7	0.929	15.7	0.097	88.98 (31)	19.03 (7)	17800	105	95.04	4.60	0.36	.00399 (2)	.0266 (7)	.0484 (12)	0.31	25.7 ± 0.1	26.7 ± 0.7
H8	0.494	30.4	0.156	119.9 (46)	20.46 (8)	25400	91.9	95.32	4.55	0.13	.00401 (1)	.0264 (4)	.0477 (7)	0.32	25.8 ± 0.1	26.4 ± 0.4

[a] Hübnerite samples are from the top of a single crystal.
[b] Lead isotope ratios are corrected for fractionation and isotopic tracer. The uncertainty of the uncorrected $^{238}U/^{204}Pb$ ratios, which is essentially the concentration ratio of U and Pb, is better than 1%. Since Pb_{blank} represents a significant contribution to Pb_{total}, all ratios involving ^{204}Pb change considerable with blank correction and are highly correlated.
[c] Lead concentration determined by isotope dilution. The reported value is the combined amount of sample Pb and blank Pb.
[d] Lead corrected for fractionation, blank, isotopic tracer, and initial lead with $^{206}Pb/^{204}Pb = 17.866$; $^{207}Pb/^{204}Pb = 15.604$, and $^{208}Pb/^{204}Pb = 38.543$. The ratios were corrected for 15 pg Pb and 1 pg U. Uncertainties at 2σ level (brackets refer to last digits) were calculated using Monte-Carlo modeling as described in the text. Rho = correlation between errors of $^{206}Pb/^{238}U$ and $^{207}Pb/^{235}U$ values.
[e] Apparent ages were calculated using the constants of Jaffey et al. (1971), recommended by IUGS (Steiger and Jäger, 1977).

$^{206}Pb/^{204}Pb$ values are even more sensitive to the common Pb correction. For instance, varying the amount of blank Pb would reduce the age of the samples with the higher $^{206}Pb/^{204}Pb$ by less than 0.1 Ma, whereas those samples with the lowest $^{206}Pb/^{204}Pb$ would be reduced by 0.4 Ma. The scatter among the apparent $^{206}Pb/^{238}U$ ages, however, does not change (Fig. 3a). It should be noted that other processes that generate scatter in $^{206}Pb/^{204}Pb$ and $^{207}Pb/^{204}Pb$ values among fragments from a single crystal cannot account for the observed scatter. Since Th is much less efficiently transported in many kinds of fluids, there may have been an initial deficit in ^{230}Th, which is an intermediate daughter in the ^{238}U decay series, eventually resulting in a ^{206}Pb deficit (e.g., Mattinson, 1973; Schärer, 1984). The maximum magnitude of this deficit is estimated using the equation of Schärer (1984). The effect corresponds to less than 130 ky, i.e., cannot account for the observed scatter. Minerals that have grown into open spaces may lose U daughters by α-recoil (e.g., Fleischer, 1980; Romer and Rocholl, 2004), which would especially affect the accumulation of ^{206}Pb. Loss of U daughters by this process is restricted to a thin veneer at the crystal surface. Because of the relatively large size of the individual fragments analyzed in this study, such a loss is not analytically resolvable. A second kind of U–Pb fractionation by α-recoil may occur when the U content of the hübnerite fragments is not hosted in the hübnerite lattice, but in U-rich micro-inclusions in hübnerite. Since the spatial distribution of parent (U, Th) and daughter (Pb) is not identical (due to α-recoil of the daughters), there may be fragments with an excess or a deficit in radiogenic Pb (cf. Mattinson et al., 1996; Romer and Thomas, 2005). U-rich phases would generate halos of radiation damage and therefore become optically distinctive. Since no halos were observed, it is unlikely that the combination of micro-inclusions and α-recoil resulted in the excess scatter of the data. Furthermore, U/Pb fractionation by α-recoil is likely to affect samples with higher U contents more strongly than those with lower U contents. Thus, the excess scatter of the data is solely due to the correction procedure for Pb_{common} and reflects the order of magnitude uncertainties may take for samples where blank and initial Pb have comparable levels and the measured $^{206}Pb/^{204}Pb$ is relatively low.

A $^{206}Pb/^{204}Pb$–$^{238}U/^{204}Pb$ isochron circumvents the problem to estimate the initial Pb isotopic composition and yields for single-stage systems accurate and precise age data as long as the isotopic composition Pb_{common} is homogeneous and Pb_{blank} is subordinate to Pb_{common}. If these requirements are not fulfilled, the data scatter in particular at the low-$^{238}U/^{204}Pb$ side of the isochron. This is shown in Fig. 3b. The data (Table 1; not corrected for Pb_{blank}) scatter significantly about the regression line that corresponds to an U–Pb age of 25.4 ± 1.1 Ma and an initial $^{206}Pb/^{204}Pb$ value of 19.1 ± 2.1 (2σ, Fig. 3b). Accounting for 15 pg blank Pb increases the $^{206}Pb/^{204}Pb$ and

$^{238}U/^{204}Pb$ values to range from 44.49 to 186.9 and from 6100 to 42,000, respectively. As the isotopic composition of Pb_{blank} and Pb_{common} is similar, blank correction essentially does not affect the slope of the regression line and, thus, the isochron age (25.4 ± 1.0 Ma, 2σ). Because of the larger spread of blank-corrected $^{238}U/^{204}Pb$ values, the age uncertainty becomes smaller even for a larger MSWD (204 vs. 60), whereas the uncertainty of the initial increases (19.2 ± 3.1). Both slope and initial are strongly influenced by the highly scattered low-$^{206}Pb/^{204}Pb$ samples. The average value of the initials is markedly higher than the Pb composition of galena form the Alma area or the Colorado Mineral Belt ($^{206}Pb/^{204}Pb$: 17.5–18.1; Stein, 1985), which suggests that the actual initial $^{206}Pb/^{204}Pb$ is lower and, concomitantly, the slope is steeper. Thus, the regression lines represent rotated mixing lines that yield minimum ages. Using the $^{207}Pb/^{204}Pb$–$^{235}U/^{204}Pb$ diagram (Fig. 3c), which is insensitive to effects of initial decay-series disequilibrium, does not change the situation considerable. The fit of the regression line to the measured values (no blank correction) shows an apparently better fit (MSWD = 4.2) than for the corresponding data in the $^{206}Pb/^{204}Pb$–$^{238}U/^{204}Pb$ diagram (MSWD = 60), but the data pattern remains the same. The apparently better fit is due to the small range in $^{207}Pb/^{204}Pb$ values relative to the analytical uncertainties. The larger relative uncertainty in $^{207}Pb/^{204}Pb$ eventually results in a less precise age (Fig. 3c).

The best age estimate is obtained from the three samples with the highest $^{206}Pb/^{204}Pb$ values. Taking uncertainties for the relative importance of blank and common Pb and for the isotopic composition of these Pb contributions into consideration, the $^{206}Pb/^{238}U$ age of hübnerite from the Sweet Home Mine is 25.7 ± 0.3 Ma (2σ).

4.2. Apatite

The Pb isotopic composition of five fragments from a single hydrothermal apatite crystal that formed during the late stage of the Sweet Home Mine mineral paragenesis, is only little radiogenic (Table 2) and, therefore, the most robust age estimate for apatite is obtained from a $^{206}Pb/^{204}Pb$–$^{238}U/^{204}Pb$ isochron (Fig. 3d). Because of the high contents of U and Pb in the various samples, blank correction has an insignificant effect on the $^{206}Pb/^{204}Pb$ and $^{238}U/^{204}Pb$ ratios. The regression line fitted through the apatite samples—if interpreted as isochron—corresponds to an age of 24.8 ± 0.5 Ma (2σ; MSWD = 1.0) with an initial $^{206}Pb/^{204}Pb$ value of 17.791 ± 0.021 (Fig. 3d).

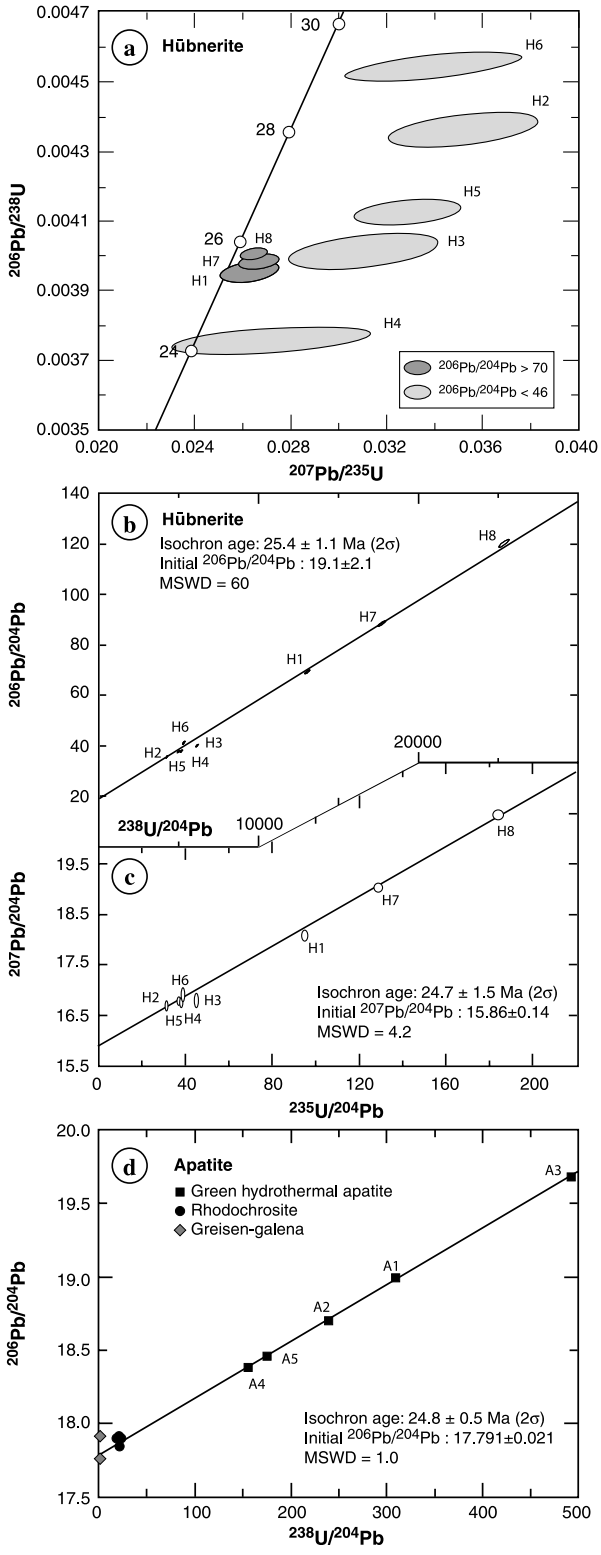

Fig. 3. (a) Concordia diagram for fragments from a single, hydrothermal hübnerite crystal. Note, that those samples with $^{206}Pb/^{204}Pb$ values above 70 fall in a cluster, whereas the scatter to younger and older apparent $^{206}Pb/^{238}U$ ages is due to samples with $^{206}Pb/^{204}Pb$ values below 46. The scatter is entirely due to the high contribution of common Pb to these latter samples and the ratio between blank Pb and initial Pb, which may differ from sample to sample. (b) $^{206}Pb/^{204}Pb$–$^{238}U/^{204}Pb$ isochron diagram for hübnerite. Note that the isochron age, which is independent on an estimate for the common Pb composition, is only slightly younger than the $^{206}Pb/^{238}U$ age, whereas the initial $^{206}Pb/^{204}Pb$ is distinctly more radiogenic than the composition of galena from the Sweet Home mine and other deposits of the Colorado Mineral Belt. Note the strong scatter at low $^{206}Pb/^{204}Pb$. (c) $^{207}Pb/^{204}Pb$–$^{235}U/^{204}Pb$ isochron diagram for hübnerite. (d) $^{206}Pb/^{204}Pb$–$^{238}U/^{204}Pb$ isochron diagram for late stage apatite. Hübnerite and apatite data from Tables 1 and 2; rhodochrosite and galena data from Romer et al. (unpublished data).

Table 2
U–Pb analytical results for apatite crystals from Sweet Home Mine, Colorado

Sample[a]	Weight (mg)	Pb[b] (ppm)	U[b] (ppm)	$^{206}Pb^{c}/^{204}Pb$	$^{207}Pb^{c}/^{204}Pb$	$^{208}Pb^{c}/^{204}Pb$	$^{238}U^{d}/^{204}Pb$	$^{206}Pb^{d}/^{238}U$	$^{206}Pb^{e}/^{238}U$
A1	29.674	5.48	26.4	18.994	15.593	38.501	309	.00389 (17)	25.0 ± 1.1
A2	36.014	1.86	6.94	18.700	15.574	38.427	238	.00380 (22)	24.4 ± 1.4
A3	36.762	1.60	12.2	19.687	15.624	38.504	492	.00385 (11)	24.8 ± 0.7
A4	33.022	7.78	18.9	18.384	15.570	38.405	154	.00383 (33)	24.7 ± 2.1
A5	33.745	6.71	18.4	18.466	15.571	38.427	174	.00385 (30)	24.8 ± 1.9

[a] All apatite samples are small fragments of individual, perfectly clear crystal.
[b] Pb and U concentration were determined by isotope dilution.
[c] Isotope ratios were corrected for 15 pg Pb blank, tracer Pb, and 0.1 %/a.m.u. mass discrimination. Note that each sample contained more than 50 ng Pb and, thus, corrections for blank and tracer Pb are insignificant.
[d] Isotope ratios were corrected for 15 pg Pb blank, tracer Pb, 1 pg U blank, and 0.1%/a.m.u. mass discrimination. The following initial Pb composition was used for data reduction: $^{206}Pb/^{204}Pb = 17.792 \pm 0.050$; $^{207}Pb/^{204}Pb = 15.542 \pm 0.030$; $^{208}Pb/^{204}Pb = 38.372 \pm 0.050$. The reported 2σ error limits for $^{206}Pb/^{238}U$ (brackets refer to last digits) were obtained from Monte-Carlo modeling as described in the text.
[e] Apparent ages calculated using the constants of Jaffey et al. (1971) recommended by IUGS (Steiger and Jäger, 1977).

This value for the initial Pb isotopic composition falls in the range known for galena and rhodochrosite from the Sweet Home mine (Romer et al., unpublished data). Including the rhodochrosite samples into the apatite data set to extend the range in $^{206}Pb/^{204}Pb$, however, makes little sense, as they may have precipitated from fluids with contrasting Pb isotopic composition. Including rhodochrosite to constrain the apatite isochron increases the scatter (MSWD = 7.3) and does not contribute to a better constrained age (24.4 ± 0.8 Ma). The age difference between apatite and hübnerite, which agrees with the textural relations, however, is difficult to quantify because of the scattered appearance of the hübnerite data.

5. Discussion

Recent $^{40}Ar/^{39}Ar$ age determinations indicate that sericite from the Sweet Home mine formed between 26.1 ± 0.1 and 25.5 ± 0.1 Ma (2σ) ago (Barbá et al., 2005), possibly indicating that earlier published K–Ar ages of 30–27 Ma for sericite (Misantoni et al., 1998) have been affected by excess argon. Furthermore, the $^{40}Ar/^{39}Ar$ ages agree closely with ages from nearby deposits, including quartz–molybdenite veinlets from the world-class Climax Mo-deposit (K/Ar on sericite, 25.5 ± 0.3 Ma (1σ), Bookstrom et al., 1988). The short $^{206}Pb/^{204}Pb$–$^{238}U/^{204}Pb$ isochron from late apatite from the Sweet Home mine yields a minimum age of 24.8 ± 0.5 Ma for the rhodochrosite and hübnerite mineralization. The $^{206}Pb/^{238}U$ age for hübnerite of 25.7 ± 0.3 Ma (2σ) falls within the expectation range of 26.1 ± 0.1 to 24.8 ± 0.5 Ma.

U–Pb dating of hübnerite can yield accurate and precise ages, even for very young samples. Because of the similarity of the ionic radii of Mn^{2+} and Fe^{2+} and the mutual substitution of these two elements in the same lattice site in wolframite-series minerals, it is quite likely that not only hübnerite is appropriate for U–Pb dating, but also ferberite. In contrast, the Ca-wolframate scheelite is less likely to be suitable for U–Pb geochronology as Pb may substitute in significant amounts for Ca.

Combined dating and fluid inclusion studies of hübnerite may be particularly useful in deposits with mineral assemblages that show systematic changes in fluid composition and that may have been deposited either from a single evolving fluid-rock system or from several hydrothermal systems widely separated in time. For instance, fluids giving rise to the Sweet Home Mine mineralization were interpreted as magmatic fluids that have been increasingly diluted (Reynolds, 1998). The arguments for this view include: (i) There are only two-phase, low-carbonic, liquid-rich aqueous inclusions present; (ii) There is no evidence for boiling; (iii) high-temperature inclusions have low to moderate salinities in the range between 2 and 4 wt% NaCl equivalent; (iv) Later, medium- and low-temperature inclusions show systematically decreasing salinity and are free of CO_2. Romer et al. (unpublished data) found evidence for boiling and phase separation during early quartz formation and demonstrated the mutual exclusive occurrence of N_2 and CO_2 in different fluid inclusions. Hübnerite is the paragenetically oldest mineral at Sweet Home that contains N_2 and reveals the involvement of a fluid that has re-equilibrated with the metamorphic wallrocks or that was derived from a meteoric source. This is in line with heterogeneous initial Pb isotopic composition, more radiogenic Sr in late minerals (Romer et al., unpublished data), and higher Fe-contents in late rhodochrosite (e.g., Wenrich, 1998). The close correspondence of the ages of hübnerite, apatite, and mica suggests that the presence of different fluid sources do not require several hydrothermal systems, but may reflect an evolving system that with progressively lower temperature sampled different fluid sources.

It is noteworthy that the emplacement of the Climax-type porphyry molybdenum deposits as for instance the Climax leucogranite and leucocratic porphyry and—farther to the north—the Henderson rhyolite stocks typically is associated with hydrothermal mineralization in the outer parts of the ore system. These hydrothermal deposits are characterized by the paragenetic sequences of W, Pb–Zn, and Mn minerals (e.g., Wallace et al., 1968; Seedorff and

Einaudi, 2004) and locally include rhodochrosite. In such a context, the Sweet Home Mine is not the only rhodochrosite producing mineralization in the Colorado Mineral Belt, but just the most famous one. In some deposits, there is a distinct metal zonation with porphyry molybdenite mineralization in the central stockwerk-type high-temperture part of the deposit and W, Pb, Zn, and Mn in the medium to low-temperature external parts. During cooling of the ore forming system, the spatial distribution of the metals may vary, eventually result in a partial overlap in the distribution of metals deposited at different temperatures (cf. Seedorff and Einaudi, 2004). The combination Re–Os dating of molydenite in the internal and (predominantly) high-temperature zones and the U–Pb dating of hübnerite from the external and medium to low-temperature zones may help to constrain the life-time of large phorphyry molybdenum deposits, particularly if formed from multiple intrusions.

6. Conclusions

The $^{206}Pb/^{238}U$ age of hübnerite ($MnWO_4$) from Sweet Home mine, Colorado, is slightly older than texturally younger apatite and closely corresponds to genetically related intrusions from the nearby Climax area. This agreement demonstrates that the U–Pb system of hübnerite can yield accurate and precise ages. Hübnerite is transparent to light in the near IR spectral range and, thus, represents one of the rare examples of a mineral suitable for both geochronological and fluid-inclusion studies. Fluid inclusion data from hübnerite of the Sweet Home mine demonstrate that hübnerite was deposited at shallow-level from a non-magmatic fluid at around 325–355 °C. Although hübnerite is rare, its occurrence in medium-temperature hydrothermal deposits—for which reliable chronometers are not too common—may make it an important mineral for the dating of some types of hydrothermal ore deposits. In particular in porphyry molydenite deposits, the combination of Re–Os dating of molydenite from the high-temperature and central sections with U–Pb dating of hübnerite from the medium-temperature and external sections may provide important constraints on the understanding of processes forming these deposits and the duration of ore formation and metal redistribution. It is speculated that ferberite ($FeWO_4$) also may represent a potentially useful mineral for U–Pb dating.

Acknowledgments

We are indebted to Bryan Lees (Collector's Edge, Golden, Colorado) for providing sample material and geological background information. We thank C. Schulz (GFZ Potsdam) for help in the laboratory and G. Berger (GFZ Potsdam) for preparing doubly polished thick sections. We gratefully acknowledge detailed and constructive reviews by Holly Stein, Fernando Corfu, and an anonymous reviewer and the thoughtful suggestions of associate editor Yuri Amelin. We are particularly grateful to Holly Stein for providing copies of papers in less accessible journals.

Associate editor: Yuri Amelin

Appendix A. Supplementary data

Supplementary data associated with this article can be found, in the online version, at doi:10.1016/j.gca.2006.07.003.

References

Bailly, L., Grancea, L., Kouzmanov, K., 2002. Infrared microthermometry and chemistry of wolframite from the Baia Sprie epithermal deposit, Romania. *Econ. Geol.* **97**, 415–423.

Barbá, K.E., Nelson, E.P., Misantoni, D., Hitzman, M.W., Layer, P.W. 2005. Structural controls on mineralized veins in the Sweet Home mine, Alma district, Colorado. In: Rhoden, H.N., Steininger, R.C., Vikre, P.G. (Eds.), *Geol. Soc. Nevada Symp. 2005*, 698–708.

Baxter, E.F. 2003. Natural constraints on metamorphic reaction rates. In: Vance, D., Müller, W., Villa, I.M. (Eds.), *Geochronology: Linking the Isotopic Record with Petrology and Textures. Geol. Soc. London Spec. Publ. 220*, 183–202.

Belyatsky, B.V., Kempe, U., Levsky, L.K., 1993. Sm–Nd age of wolframite from quartz–wolframite ore occurrences o Saxony, Germany. *Terra Abstr.* **5** (Suppl. 1), 442–443.

Bookstrom, A.A., Carten, R.B., Shannon, J.R., Smith, R.P., 1988. Origins of bimodal leucogranite–lamprophyre suites, Climax and Red Mountain porphyry molybdenum systems, Colorado: petrologic and strontium isotopic evidence. *Colo. Sch. Mines Q.* **83**, 1–24.

Burton, K.W., O'Nions, R.K., 1991. High-resolution garnet chronometry and the rates of metamorphic processes. *Earth Planet. Sci. Lett.* **107**, 649–671.

Christensen, J.N., Rosenfeld, J.L., DePaolo, D.J., 1989. Rates of tectonometamorphic processes from rubidium and strontium isotopes in garnet. *Science* **244**, 1465–1469.

Duchène, S., Lardeaux, J.-M., Albarède, F., 1997. Exhumation of eclogites: insights from depth-time path analysis. *Tectonophysics* **280**, 125–140.

Cerny, P., Ercit, T.C., 1989. Mineralogy of niobium and tantalum: crystal chemical relationships, paragenetic aspects and their economic implications. In: Möller, P., Cerny, P., Saupé, F. (Eds.), *Lanthanides, Tantalum and Niobium*. Springer-Verlag, Berlin Heidelberg, pp. 27–79.

Fleischer, R.L., 1980. Isotopic disequilibrium of uranium alpha-recoil damage and preferential solution effect. *Science* **207**, 979–981.

Franzke, H.J., Ahrend, H., Kurz, S., Wemmer, K., 1996. K–Ar Datierungen von Illiten aus Kataklasiten der Flossbergstörung im südöstlichen Thüringer Wald und ihre geologische Interpretation. *Z. Geol. Wiss.* **24**, 441–456.

Jaffey, A.H., Flynn, K.F., Glendenin, L.E., Bentley, C., Essling, A.M., 1971. Precision measurement of half-lives and specific activities of ^{235}U and ^{238}U. *Phys. Rev.* **C4**, 1889–1906.

Jhaveri, J., Robinson, D.B., 1965. Hydrates in the methane–nitrogen system. *Can. J. Chem. Eng.* **43**, 75–78.

Kontak, D.L., Archibald, D.A., 2002. $^{40}Ar/^{39}Ar$ dating of hydrothermal biotite from high-grade gold ore, Tangier gold deposit, Nova Scotia; further evidence for 370 Ma gold metallogeny in the Meguma Terrane. *Econ. Geol.* **97**, 619–628.

Lüders, V., 1996. Contribution of infrared microscopy to fluid inclusion studies in some opaque minerals (wolframite, stibnite, bournonite); metallogenic implications. *Econ. Geol.* **91**, 1462–1468.

Lüders, V., Romer, R.L., Cabral, A.R., Schmidt, C., Banks, D.A., Schneider, J., 2005. Genesis of itabirite-hosted Au–Pd–Pt-bearing hematite–(quartz) veins, Quadrilátero Ferrífero, Minas Gerais, Brazil: Constraints from fluid inclusion infrared microthermometry, bulk

crush-leach analysis and U–Pb systematics. *Miner. Deposita* **40**, 289–306.

Macfarlane, A.W., Tosdal, R.M., Vidal, C.E., Paredes, J. 1999. Geologic and isotopic constraints on the age and origin of auriferous quartz veins in the Parcoy mining district, Pataz, Peru. In: Skinner, B.J. (Ed.), *Geology and Ore Deposits of the Central Andes. Econ. Geol. Spec. Publ.* **7**, 267–279.

Mattinson, J.M., 1973. Anomalous isotopic composition of lead in young zircons. *Carnegie Inst. Wash. Yearbook* **72**, 613–616.

Mattinson, J.M., Gaubard, C.M., Parkinson, D.L., McLelland, W.C., 1996. U–Pb reverse discordance in zircons: the role of fine-scale oscillatory zoning and sub-microscopic transport of Pb. *Am. Geophys. Union Geophys. Monogr.* **95**, 355–370.

Moore, T., 1998. New operations at the Sweet Home Mine 1990-1997. *Mineral. Rec.* **29**, 21–100.

Murphy, J.A., Hurlbut, J.F., 1998. Minerals of the Sweet Home Mine. *Mineral. Rec.* **29**, 115–122.

Misantoni, D., Silberman, M.L., Lees, B.K., 1998. Geology of the Sweet Home Mine and the Alma district. *Mineral. Rec.* **29**, 101–114.

Möller, A., O'Brien, P.J., Kennedy, A., Kröner, A. 2003. Linking growth episodes of zircon and metamorphic textures to zircon chemistry: an example from the ultrahigh-temperature granulites of Rogaland (SW Norway). In: Vance, D., Müller, W., Villa, I.M. (Eds.), *Geochronology: Linking the Isotopic Record with Petrology and Textures. Geol. Soc. Lond. Spec. Publ.* **220**, 65–81.

Neymark, L.A., Amelin, Y.V., Paces, J.B., 2000. ^{206}Pb–^{230}Th–^{234}U–^{238}U and ^{207}Pb–^{235}U geochronology of Quaternary opal, Yucca Mountain, Nevada. *Geochim. Cosmochim. Acta* **64**, 2913–2928.

Nie, F., Jiang, S., Bai, D., Liu, Y., Zhao, X., 2002. Sm/Nd isotope age of wolframite from the Shachang rapakivi granitic intrusive complex, Miyun County, Beijing, China. *Geol. Rev.* **48**, 29–33.

Pettke, T., Diamond, L.W., 1995. Rb-Sr isotopic ananlysis of fluid inclusions in quartz: evaluation of bulk extraction procedures and geochronometer systematics using synthetic fluid inclusions. *Geochim. Cosmochim. Acta* **59**, 4009–4027.

Pettke, T., Diamond, L.W., 2000. Rb–Sr dating of Sphalerite based on fluid inclusion-host mineral isochrons: a clarification of why it works. *Econ. Geol.* **91**, 951–956.

Reynolds, T.J., 1998. Sweet Home rhodochrosite—What makes it so cherry red? *Mineral. Rec.* **29**, 127–132.

Romer, R.L., 2001. Lead incorporation during crystal growth and the misinterpretation of geochronological data from low-$^{238}U/^{204}Pb$ metamorphic mineral. *Terra Nova* **13**, 258–263.

Romer, R.L., Linnemann, U., 2004. U–Pb dating the Schlottwitz agate-amethyst vein (Erzgebirge, Saxony). *Eur. J. Mineral.* **16** (Beiheft 1), 116.

Romer, R.L., Lüders, V., Gilg, H.A., Pettke, T., Misantoni, D. (unpublished data). The sweet home mine (Alma, Colorado)—a poor cousin of the giant climax molybdenum deposit.

Romer, R.L., Rocholl, A., 2004. Activity disequilibrium of ^{230}Th, ^{234}U, and ^{238}U in old stilbite: effects of young U mobility and α-recoil. *Geochim. Cosmochim. Acta* **68**, 4705–4719.

Romer, R.L., Rötzler, J., 2001. P–T–t evolution of ultrahigh-temperature granulites from the Saxon Granulite Massif, Germany. Part II: Geochronology. *J. Petrol.* **42**, 2015–2032.

Romer, R.L., Rötzler, J. 2003. Effect of metamorphic reaction history on the U–Pb dating of titanite. In: Vance, D., Müller, A., Villa, I. (Eds.), *Geochronology: Linking the Isotopic Record with Petrology and Textures. Geol. Soc. Lond. Spec. Publ.* **220**, 147–158.

Romer, R.L., Siegesmund, 2003. Why allanite may swindle about its true age. *Contrib. Mineral. Petrol.* **146**, 297–307.

Romer, R.L., Thomas, R. 2005. U–Pb dating of micro-inclusions: the age of the Ehrenfriedersdorf tin deposit (Erzgebirge, Germany). In: Mao Jingwen, Bierlein, F.P. (Eds.), *Mineral Deposits Research: Meeting the Global Challenge. Proceedings 8th Biennial SGA Meeting Beijing, China, 18–21 August 2005*, pp. 817–820.

Romer, R.L., Xiao, Yilin, 2005. Initial Pb–Sr(–Nd) isotopic heterogeneity in a single allanite–epidote crystal: implications of reaction history for the dating of minerals with low parent-to-daughter ratios. *Contrib. Mineral. Petrol.* **148**, 662–674.

Romer, R.L., Heinrich, W., Schröder-Smeibidl, B., Meixner, A., Fischer, C.-O., Schulz, C., 2005a. Elemental dispersion and stable isotope fractionation during reactive fluid-flow and fluid immiscibility in the Bufa del Diente aureole, NE-Mexico: evidence from radiographies and Li, B, Sr, Nd, and Pb isotope systematics. *Contrib. Mineral. Petrol.* **149**, 400–429.

Romer, R.L, Lüders, V., Banks, D.A., Schneider, J. 2005b. U–Pb data of Au–Pd–Pt-bearing quartz–hematite veins, Quadrilátero Ferrífero, Minas Gerais, Brazil. In: Mao Jingwen, Bierlein, F.P. (Eds.), *Mineral Deposits Research: Meeting the Global Challenge. Proceedings 8th Biennial SGA Meeting Beijing, China, 18–21, August 2005*, pp. 821–824.

Schärer, U., 1984. The effect of initial 230Th disequilibrium on young U–Pb ages: the Makalu case, Himalaya. *Earth Planet Sci. Lett.* **67**, 191–204.

Seedorff, E., Einaudi, M., 2004. Henderson Porphyry molydenum system, Colorado: II. Decoupling of introduction and deposition of metals during geochemical evolution of hydrothermal fluids. *Econ. Geol.* **99**, 39–72.

Shannon, R.D., 1976. Revised effective ionic radii and systematic studies of interatomic distances in halides and chalcogenides. *Acta Cryst.* **32**, 751–767.

Steiger, R.H., Jäger, E., 1977. Subcommission on geochronology: convention on the use of decay constants in geo- and cosmochronology. *Earth Planet. Sci. Lett.* **36**, 359–362.

Stein, H.J. 1985. A lead, strontium, sulfur isotope study of Laramide-Tertiary intrusions and mineralization in the Colorado Mineral Belt with emphasis on Climax-type porphyry molybdenum systems plus a summary of other newly acquired isotopic and rare earth element data. Ph.D. Diss., Univ. North Carolina, Chapel Hill, 493 pp.

Vance, D., O'Nions, R.K., 1990. Isotopic chronometry of zoned garnets: growth kinetics and metamorphic histories. *Earth Planet. Sci. Lett.* **97**, 227–240.

Wallace, S.R., Muncaster, N.K., Jonson, D.C., Mackenzie, W.B., Bookstrom, A.A., Surface, V.E. 1968. Multiple intrusion and mineralization at Climax, Colorado. In: Ridge, J.D. (Ed.), *Ore Deposits of the Unites States, 1933–1967 (Graton-Sales Volume). Am. Inst. Min. Met. Pet. Eng.*, 605–640.

Wenrich, K.J., 1998. Sweet Home rhodochrosite—What makes it so cherry red? *Mineral. Rec.* **29**, 123–127.

Wernicke, R.S., Lippolt, H.J., 1993. Botryoidal hematite from the Schwarzwald (Germany): heterogeneous uranium distributions and their bearing on the helium dating method. *Earth Planet. Sci. Lett.* **114**, 287–300.

Wernicke, R.S., Lippolt, H.J., 1994. 4He age discordance and release behavior of a double shell botryoidal hematite from the Schwarzwald (Germany). *Geochim. Cosmochim. Acta* **58**, 421–429.

Wood, S.A., Samson, I.M., 2000. The hydrothermal geochemistry of tungsten in granitoid environments; I, relative solubilities of ferberite and scheelite as a function of T, P, pH, and m_{NaCl}. *Econ. Geol.* **95**, 143–182.